Knyazeva A.G., Korosteleva E.N., Safronova V.S. Sintering and thermokinetic modeling ...



Theory and Processes of Formation and Sintering of Powder Materials Теория и процессы формования и спекания порошковых материалов



UDC 536.421.5

https://doi.org/10.17073/1997-308X-2025-5-5-16

Research article Научная статья



Sintering and thermokinetic modeling of the phase evolution in thermite powder mixtures under controlled heating

A. G. Knyazeva, E. N. Korosteleva, V. S. Safronova

Institute of Strength Physics and Materials Science, Siberian Branch, Russian Academy of Sciences 8/2 Akademicheskii Prosp., Tomsk 634055, Russia

19627826013@yandex.ru

Abstract. The behavior of compacted mixtures of metal powders (Al, Ti) and recycled metalworking wastes (Fe + Fe₂O₃ + C) during vacuum sintering under controlled heating was investigated to assess the possibility of producing in situ metal—matrix composites containing oxide strengthening particles. The starting materials were titanium and aluminum powders (particle size <160 μm and <100 μm, respectively) and a powder produced from recycled steel chips (<300 μm). The resulting samples exhibited a heterogeneous phase composition, which was examined by *X*-ray diffraction (CuK_α radiation, XRD-6000 diffractometer) and optical microscopy (Axiovert 200MAT). A pronounced difference was observed between the aluminum- and titanium-based systems: the former exhibited a distinct thermal peak, whereas the latter showed smooth temperature behavior without thermal spikes. A thermokinetic model describing the multi-stage reactions in both systems was developed. The model incorporates metallothermic reduction and intermetallic formation reactions. Formal kinetic parameters were estimated using a semi-empirical approach and refined by comparison with experimental data. The governing equations, including the heat balance equation and the system of kinetic rate equations, were solved numerically using a semi-implicit Euler method, while mass conservation and atomic balance were verified. The initial composition of the samples was varied in the calculations – accounting for oxygen, carbon, and the Fe/Fe₂O₃ ratio in the steel-chippowder – to reproduce the experimentally observed product compositions. The calculated and experimental results showed qualitative agreement.

Keywords: metal-matrix composite, vacuum sintering, metallothermic reactions, intermetallics, thermokinetic model

Acknowledgements: This work was carried out within the framework of the Fundamental Research Program of the Institute of Strength Physics and Materials Science, Siberian Branch of the Russian Academy of Sciences (ISPMS SB RAS): Project FWRW-2022-0003 (theoretical part) and Project FWRW-2021-0005 (experimental part).

For citation: Knyazeva A.G., Korosteleva E.N., Safronova V.S. Sintering and thermokinetic modeling of the phase evolution in thermite powder mixtures under controlled heating. *Powder Metallurgy and Functional Coatings*. 2025;19(5):5–16. https://doi.org/10.17073/1997-308X-2025-5-5-16



Спекание и термокинетическое моделирование эволюции состава термитных смесей в условиях регулируемого нагрева

А. Г. Князева, Е. Н. Коростелева, В. С. Сафронова

Институт физики прочности и материаловедения Сибирского отделения РАН Россия, 634055, г. Томск, пр. Академический, 8/2

№ 19627826013@yandex.ru

Аннотация. Проанализировано поведение прессовок из смесей порошков металлов (Al, Ti) и переработанных отходов металлообработки (Fe + Fe₂O₃ + C) в условиях вакуумного спекания при регулируемом нагреве для исследования возможности получения in situ металломатричных композиционных материалов с упрочняющими оксидными частицами. В качестве исходных материалов использованы порошки титана и алюминия с фракциями d < 160 мкм и < 100 мкм соответственно, а также порошок переработанной стружки из стали размером менее 300 мкм. В результате проведенного эксперимента обнаружен неоднородный фазовый состав образцов, который исследовали с помощью рентгеновского дифрактометра XRD-6000 с CuK_a-излучением и оптического микроскопа «Axiovert 200MAT». Продемонстрировано существенное различие в поведении систем на основе алюминия и титана: первая система характеризуется ярко выраженным термическим пиком, а во второй - превращения идут в спокойном режиме. Предложена термокинетическая модель процесса, учитывающая стадийность превращений для обеих систем. Учтены металлотермические реакции и реакции образования интерметаллидов. Дана оценка формально-кинетическим параметрам реакций с помощью полуэмпирического подхода. Полученные параметры корректировались при сравнении с экспериментом. Модель реализована численно с помощью полунеявного метода Эйлера. Проверялись закон сохранения массы и неизменность числа атомов. Начальный состав образцов в расчетах варьировался (за счет учета присутствия кислорода, углерода и соотношения железа и оксида железа в стружке) таким образом, чтобы в результате синтеза получить состав продуктов, максимально приближенный к результатам эксперимента. Получено качественное соответствие теории и эксперимента.

Ключевые слова: металломатричный композит, вакуумное спекание, металлотермические реакции, интерметаллиды, термокинетическая модель

Благодарности: Работа выполнена по программе фундаментальных научных исследований ИФПМ СО РАН: проекты FWRW-2022-0003 (теоретическая часть) и FWRW-2021-0005 (экспериментальная часть).

Для цитирования: Князева А.Г., Коростелева Е.Н., Сафронова В.С. Спекание и термокинетическое моделирование эволюции состава термитных смесей в условиях регулируемого нагрева. *Известия вузов. Порошковая металлургия и функциональные покрытия*. 2025;19(5):5–16. https://doi.org/10.17073/1997-308X-2025-5-5-16

Introduction

The in-situ formation of strengthening particles in metal-matrix composites (MMCs) has become a focal point in powder-processing technologies owing to applications across the aerospace, automotive, and energy sectors, and it continues to attract sustained interest from diverse research groups [1–4]. The spectrum of MMCs obtainable by powder routes is broad – in terms of both matrix chemistries and sets of strengthening phases. Of particular interest are systems built from chemically reactive powder components, where reactions between constituents synthesize the strengthening phases in-situ as micronscale inclusions. This is largely characteristic of combustion-synthesis routes that rely on metallothermic reactions [5–9]. Such reactions are typically strongly exothermic, which helps sustain the synthesis process. Creating the strengthening particles directly during composite fabrication is advantageous for interfacial bonding with the surrounding matrix. However, when a mixture permits metallothermic reduction (one metal reducing another), the presence of additional constituents can markedly redirect reaction pathways because local interaction conditions vary across different regions of the compact [10].

The problem becomes even less straightforward if one component of the powder mixture is itself a complex material – namely, a metallic base containing oxide inclusions – produced by recycling steel chips [11].

Here, the feasibility of producing metal–matrix composites from Al–Fe₂O₃–Fe and Ti–Fe₂O₃–Fe powder mixtures (optionally containing carbon) under sintering in a vacuum chamber is assessed, together with a theoretical description based on a thermokinetic model that accounts for the kinetics of the principal reactions.



1. Experimental

1.1. Materials and methods

Phase evolution under vacuum sintering with a controlled heating program (sintering temperature 1173-1473 K; 60-min hold) was examined for powder systems based on Ti-Al-Fe₂O₃/(Fe + C) using the following representative mixtures (from several possible combinations): Al + (Fe + Fe₂O₃ + C) and Ti + (Fe + Fe₂O₃ + C). Titanium powder TPP-8 (main fraction $d < 160 \,\mu\text{m}$) and aluminum powder PA-4 $(d < 100 \mu m)$ were used to prepare the mixtures. As an analogue of the Fe + Fe₂O₂ + C composition, a powder produced from recycled steel 45 chips with a particle size not exceeding 300 µm was employed; its characteristics are described in detail in [11]. The component ratios in the mixtures were calculated to be sufficient both for metallothermic reduction and for intermetallic formation. The quantitative compositions of the powder mixtures under study are given in Table 1.

Selection of proportions for the aluminum-containing mixtures was guided by the binary Al–Fe phase diagram. The first option corresponds to the α -AlFe field, while the second lies predominantly in the Al₃Fe/AlFe phase region. Both options imply exothermic reactions.

The titanium-containing mixture comprised 75 wt. % Ti and 25 wt. % steel chips, which favors the formation of a matrix basis in the resulting composite as a solid solution of iron and oxygen in titanium.

Microstructural characterization was performed by optical microscopy, scanning electron microscopy (SEM), and X-ray diffraction (XRD). The following instruments were used: Axiovert 200MAT optical microscope (Carl Zeiss, Germany), Mira 3 LMU SEM (Tescan, Czech Republic), and XRD-600 (Shimadzu, Japan) and DRON-8 (Russia) diffractometers with CuK_{α} radiation. Phase identification employed the PDF-4+ database and POWDER CELL 2.4 for full-profile analysis.

According to [11], chips oxidized in water and then milled form oxide-coated steel-chip fragments with an Fe core, containing dissolved carbon (\approx 1.5 wt. %).

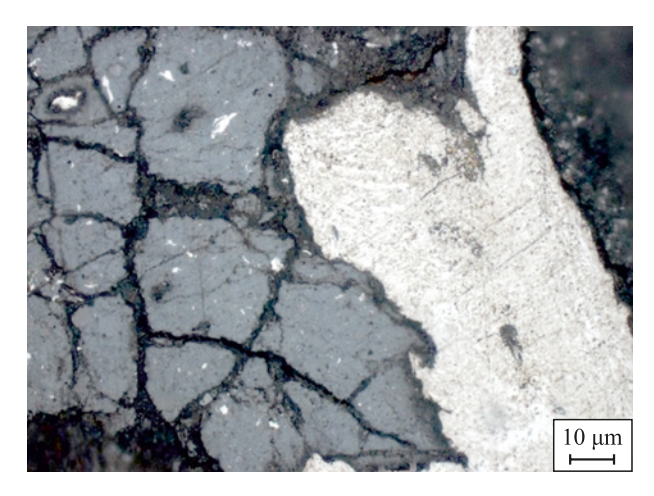


Fig. 1. Microstructure of the recycled steel 45 chips after oxidation and crushing

Light areas correspond to the steel core, dark areas to the iron oxide layer

Рис. 1. Микроструктура переработанной стружки из стали 45 после процедур окисления и дробления

Светлая область – стальная сердцевина, темная – слой из оксилов железа

Although carbide phases were not detected by XRD, the presence of carbon in the steel-chip particles was confirmed by energy-dispersive X-ray spectroscopy (EDS). Carbon content, measured with a LECO ONH-836 gas-impurity analyzer (USA), showed broad distribution (0.8–1.6 wt. %), reflecting the substantial heterogeneity of the processed steelchip-derived particles. Their surfaces bear iron-oxide regions (Fe₂O₄/Fe₂O₂/FeO) [11], with the oxide fraction reaching \approx 50–70 %. Because these oxide layers are highly nonuniform (Fig. 1), the contact between a chip-derived particle and Al or Ti powder depends on the local surface domain encountered. Within the same mixture, the second component can therefore contact metallic iron (carbon steel) and iron oxides simultaneously.

1.2. Experimental results

Under vacuum sintering at $T_s = 1273$ K, a heterogeneous phase assemblage was identified for both Al + (Fe + Fe₂O₃ + C) formulations [12]. The pressed compacts of aluminum powder with milled, oxidized

Table 1. Composition of the investigated powder mixtures, wt. % Таблица 1. Состав исследуемых порошковых смесей, мас. %

| Mixture | Composition | Ti | Al | Recycled steel chips $(Fe + Fe_2O_3 + C)$ |
|---------|---------------------------|----|----|---|
| 1 | $Al + (Fe + Fe_2O_3 + C)$ | _ | 25 | 75 |
| | | _ | 60 | 40 |
| 2 | $Ti + (Fe + Fe_2O_3 + C)$ | 75 | _ | 25 |

steel chips lost structural integrity and disintegrated into separate fragments. The selected sintering conditions were sufficient to initiate a cascade of reactions, yielding Fe–Al intermetallics together with oxide strengthening particles. Residual (unreacted) iron was also detected in the products (Fig. 2). Oxygen was transferred almost entirely from the iron oxides to aluminum, forming Al₂O₃, and FeAl constituted the dominant volumetric fraction of the product.

With increasing aluminum content in the compact, the reaction products contained a substantial fraction of residual, unreacted constituents, attributable to a decrease in the overall exothermicity of the reactions.

The second formulation, $Ti + (Fe + Fe_2O_3 + C)$, is less exothermic. Since the solubility of iron in β -Ti reaches 22 at. % at $T_s = 1358$ K and drops to 0.34 at. % in α-Ti at 673 K, it was expected that part of the iron would react with titanium to form intermetallics. It was also anticipated that titanium would be sufficient to interact with oxide inclusions present in the recycled steel-chip powder. Experimentally, the steel-chip powder in the Ti + (Fe + Fe₂O₃ + C) mixture exhibited good sinterability, with predominantly diffusional interaction with iron and oxygen migration from iron oxides into the titanium matrix. It is plausible that carbon contained in the chips enhances sintering via diffusion into titanium; however, its amount is too low to produce titanium carbide at levels detectable by X-ray diffraction. Interaction of free iron with titanium in the presence of oxide inclusions does not impede interdiffusion. The phase set and phase fractions depend on the sintering temperature; nevertheless, in all cases the pro-

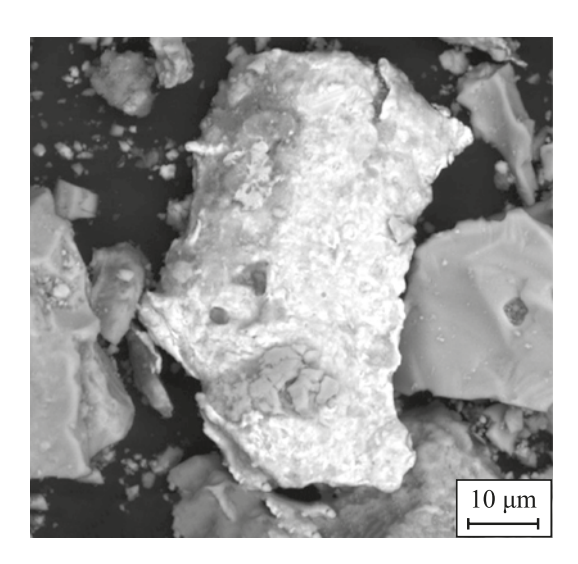
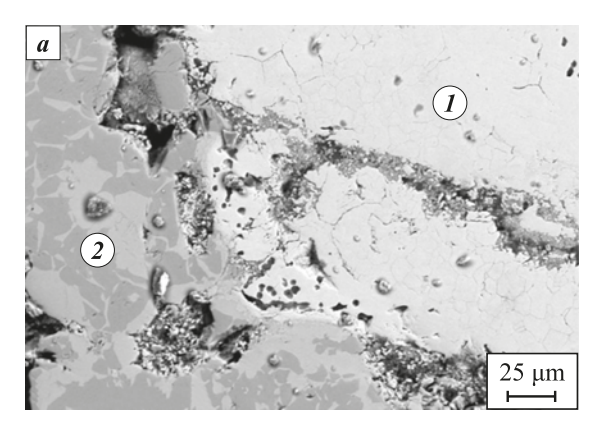


Fig. 2. Microstructure of a fragment of the sintered material $25 \% \text{Al} + 75 \% \text{ (Fe} + \text{Fe}_2\text{O}_3 + \text{C)}$

Рис. 2. Микроструктура фрагмента спеченного материала 25 % Al + 75 % (Fe + Fe₂O₃ + C)

ducts are dominated by a titanium-based solid solution (Fig. 3). At lower temperatures, the products contain a nonstoichiometric TiO_2 -based oxide (18 wt. %) and residual Fe_2O_3 (32 wt. %) originating from the steelchip particles. Iron from these particles reacts with titanium to yield up to 20 wt. % of the equiatomic intermetallic TiFe. At a higher sintering temperature (1473 K), no unreacted constituents remain, and two types of α -Ti-based solid solutions form with different dissolved Fe and O contents; small inclusions of Ti_2Fe , $TiFe_2$, or TiFe are also observed. Oxides are not detected as a separate phase under these conditions (Fig. 3).

The results reported in [13; 14] provided the basis for constructing thermokinetic models that capture the staged nature of phase formation.



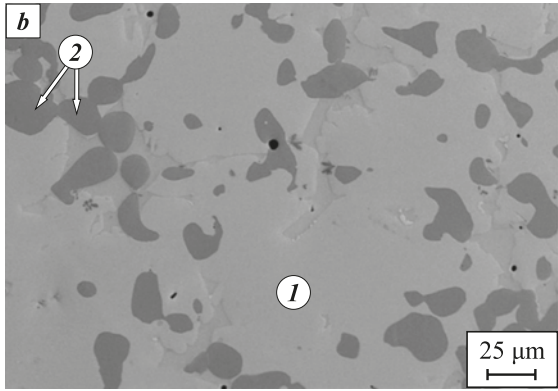


Fig. 3. Microstructure of sintered compacts from the mixture 75 % Ti + 25 % (Fe + Fe₂O₃ + C) at temperatures $T_{\rm s} = 1173$ K (a) and 1473 K (b)

a: 1 – regions of residual iron with oxide inclusions; $2 - \alpha$ -Ti of variable composition with TiFe inclusions; b: $1 - \alpha$ -Ti of variable composition with dissolved iron and oxygen, with small TiFe₂ or TiFe inclusions;

 $2 - \alpha$ -Ti regions depleted in iron with small of Ti₂Fe inclusions

Рис. 3. Микроструктура спеченных прессовок из смеси 75 % Ti + 25 % (Fe + Fe $_2$ O $_3$ + C) при температурах T_s = 1173 K (\boldsymbol{a}) и 1473 K (\boldsymbol{b})

a: I — область остатков железа с оксидными включениями; 2 — α -Ті переменного состава с включениями ТіFe; b: I — α -Ті переменного состава с растворенными железом и кислородом, небольшими включениями ТіFe $_2$ или ТіFe; 2 — области α -Ті, обедненные железом с небольшими включениями Ті,Fe



2. Sintering model with detailed kinetics

2.1. Heat balance

The thermokinetic model accounts for the sample temperature change arising from the controlled external heating program and from heat release by chemical reactions. Owing to the small sample size, temperature gradients within the compact are neglected (a lumped-capacitance assumption); estimates justifying this approximation are given in [15]. The heat-balance equation has the form

$$Vc\rho \frac{dT}{dt} = VW_{ch} + \sigma \varepsilon S \left(T_W^4 - T^4\right) - \alpha S \left(T - T_e\right), \quad (1)$$

where T is the temperature; t is time; V and S are the compact volume and surface area; c and ρ are the heat capacity and density of the pressed powder mixture; $W_{\rm ch}$ is the total heat release due to chemical reactions; σ is the Stefan-Boltzmann constant; ε is the surface emissivity of the compact; α is the heat-transfer coefficient (in vacuum it may be taken as zero); T_e is the ambient temperature (if Newton cooling is included).

The vacuum-chamber wall temperature $T_{\it W}$ follows a linear law:

$$T_W = T_0 + at$$
, for $T < T_s$,

and

$$T_w = T_s$$
, for $T \ge T_s$, (2)

where a is the heating rate and T_s is the sintering temperature.

Within the interval $T_{\rm min}$ - $T_{\rm max}$, melting is assumed to occur, with the liquid-phase fraction $(\eta_{\rm L})$ varying from 0 to 1:

$$\begin{split} \eta_{\rm L} &= 0 \quad \text{for} \quad T \leq T_{\rm min}, \\ \eta_{\rm L} &= \left(\frac{T - T_{\rm min}}{T_{\rm max} - T_{\rm min}}\right)^2 \quad \text{for} \quad T_{\rm min} < T \leq T_{\rm max}, \\ \eta_{\rm L} &= 1 \quad \text{for} \quad T > T_{\rm max}. \end{split} \tag{3}$$

Here, $T_{\rm min}$ is the lowest melting temperature among the reagents and reaction products in the chosen system, and $T_{\rm max}$ is the highest one (see Table 2).

Within the melting interval, the (specific) heat capacity is given by

$$c = \left(c_{\rm S} + \frac{Q_{\rm eff}}{m} \frac{\partial \eta}{\partial T}\right) (1 - \eta_{\rm L}) + c_{\rm L} \eta_{\rm L}, \tag{4}$$

Table 2. Melting points of the starting substances and selected reaction products

Таблица 2. Температуры плавления исходных веществ и некоторых продуктов

| Phase (compound) | T_m , K | Phase (compound) | T_m , K | |
|------------------|-----------|----------------------------------|-----------|--|
| Al | 903,3 | Ti–Al* | 1513–1733 | |
| Fe | 1811 | Ti–Fe* | 1273-1723 | |
| Ti | 1941 | Al–Fe* | 825–1583 | |
| Fe_2O_3 | 1838 | FeAl ₂ O ₄ | 1713 | |
| Al_2O_3 | 2345 | Ti ₃ FeO ₂ | _** | |
| TiO ₂ | 2116 | TiC | 3473 | |

^{*} Intermetallic phases in the corresponding binary system.

where $c_{\rm S}$ is the heat capacity of the mixture in the solid state, $c_{\rm L}$ is the heat capacity of the mixture in the liquid state; $Q_{\rm eff}$ is the effective enthalpy of fusion (J/mol); m is the mean molar mass of the mixture of reagents and reaction products.

Heat release from chemical reactions is given by

$$W_{\rm ch} = \sum_{i=1}^{n} Q_i \Phi_i, \tag{5}$$

where n is the number of reactions; Φ_i are the reaction rates; Q_i are the reaction enthalpies (heat effects).

2.2. Model of phase composition evolution during sintering

Because the detailed mechanisms of most solidstate reactions are rarely known and the steps involved often comprise a mix of physicochemical processes, it is most appropriate to use a reduced-chemistry model that explicitly tracks the formation of the experimentally observed phases.

In the Al-containing system (where aluminum has the lowest melting temperature), the dominant exothermic step is expected to be the aluminothermic reduction of iron oxide:

$$2Al + Fe2O3 = Al2O3 + 2Fe.$$
 (I)

The reduced iron then reacts with excess aluminum to form intermetallic phases. Owing to the large reaction enthalpies, phase formation is expected to occur predominantly in the liquid phase and to be accompanied by the appearance of agglomerates [16]. At the same time, as noted in [17], direct reaction

system. ** An unstable compound that decomposes before melting (at T = 1273 K).

between aluminum and iron oxides during combustion is preceded by the partial decomposition sequence $Fe_2O_3 \rightarrow Fe_3O_4 \rightarrow FeO$. Thin plates of $FeAl_2O_4$, have been observed in [17] as a result of the interaction between FeO and the amorphous Al_2O_3 film that invariably coats aluminum:

$$FeO + Al_2O_3 \rightarrow FeAl_2O_4$$
. (II)

Iron aluminates such as $FeAl_2O$ and $FeAl_2O_4$ commonly appear in the $Al-Fe_2O_3$ system, which is unfavorable for further reduction of iron oxides – especially in the presence of Al_2O_3 [18].

In the $Al-Fe_2O_3$ system, an additional step may occur

$$2\text{Fe}_2\text{O}_3 \rightarrow 4\text{FeO} + \text{O}_2$$
 (III)

followed by oxidation of aluminum:

$$4Al + 3O_2 = 2Al_2O_3.$$
 (IV)

The Al–Fe phase diagram contains several intermetallic phases (Fig. 4). The diagram was constructed using the Thermo-Calc Software (open version) with the TCBIN: TC Binary Solutions v1.1 database.

Formation of intermetallic phases proceeds via the reactions

$$Al + Fe = FeAl, (V)$$

$$FeAl + Al = FeAl_2,$$
 (VI)

$$FeAl + 2Fe = Fe_2Al,$$
 (VII)

$$FeAl_2 + Al = FeAl_3,$$
 (VIII)

$$FeAl_2 + FeAl_3 = Fe_2Al_5.$$
 (IX)

The FeAl intermetallic is not shown on the diagram; however, it is known to form by ordering of the α -Fe(Al) solid solution. Fe₃Al is a metastable phase that appears via a second-order phase transformation from FeAl [19]. Carbon present in the processed chips could, in principle, participate in the synthesis of aluminum carbide (Al₄C₃), but the sintering schedule and mixture composition do not provide sufficient carbon or temperature to initiate the corresponding reaction.

In the second case (Ti-Fe₂O₃-Fe-C system), iron is the lowest-melting component (see Table 2). According to [20], the thermite reaction Ti-Fe₂O₃ proceeds through several steps – reduction of Fe₂O₃ by Ti to form Fe and TiO₂, followed by the formation of the metastable intermetallic Ti₂Fe. Allowing for partial decomposition of iron oxide, the presence of carbon, and the formation of intermetallic phases (Fig. 4, *b*), the reaction set can be written as:

$$3Ti + 2Fe_2O_3 = 3TiO_2 + 4Fe,$$
 (I')

$$Ti + Fe = TiFe,$$
 (II')

$$TiFe + Ti = Ti_{2}Fe,$$
 (III')

$$TiFe + Fe = TiFe_{2},$$
 (IV')

$$Ti + C = TiC,$$
 (V')

$$2\text{Fe}_2\text{O}_3 \rightarrow 4\text{FeO} + \text{O}_2,$$
 (VI')

$$Ti + O_2 = TiO_2,$$
 (VII')

$$TiO_2 + Ti_2Fe = Ti_3FeO_2.$$
 (VIII')

The notation for species concentrations (C_k) for each system is given in Tables 3 and 4.

For each reaction network, the kinetic equations can be written as

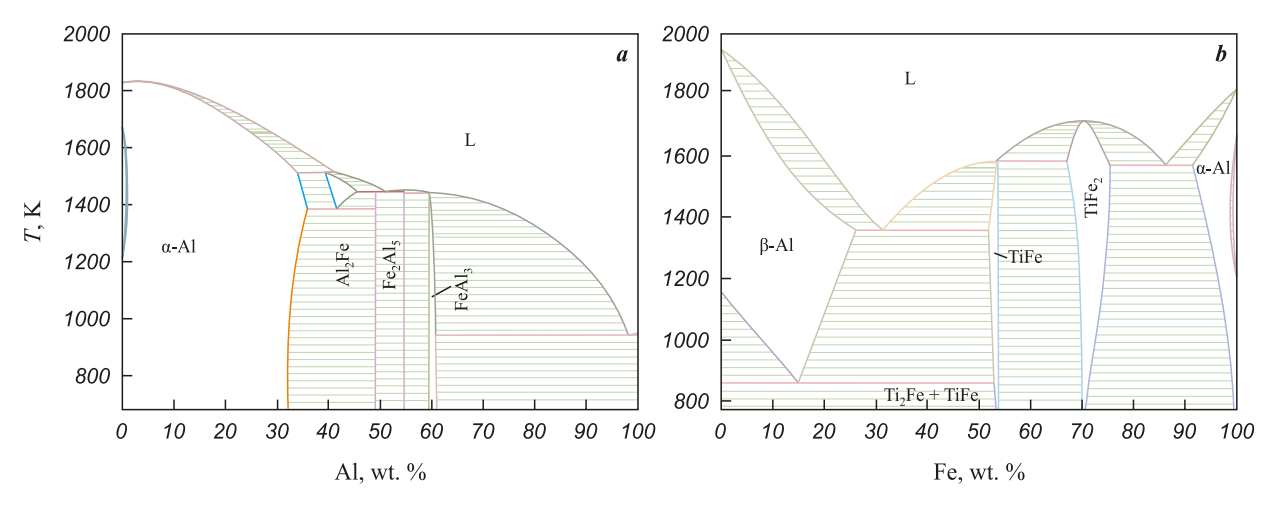


Fig. 4. Phase diagrams of the Al–Fe (a) and Ti–Fe (b) systems

Рис. 4. Диаграммы состояния Al–Fe (a) и Ti–Fe (b)

Knyazeva A.G., Korosteleva E.N., Safronova V.S. Sintering and thermokinetic modeling ...

$$\frac{dC_k}{dt} = \sum_{k=1}^r v_{ki} \Phi_i, \tag{6}$$

where v_{ki} are the stoichiometric coefficients of component k in reaction i; r is the number of reactions, Φ_i are the reaction rates. We assume that the reaction rates follow an Arrhenius temperature dependence and depend on concentrations according to the law of mass action:

$$\Phi_i = k_i(T) \prod_k C_k^{n_{ki}}. \tag{7}$$

Here, n_{ki} are the exponents equal in absolute value to the corresponding stoichiometric coefficients;

$$k_i = k_{i0} \exp\left(-\frac{E_i}{RT}\right),\tag{8}$$

where k_{i0} are the pre-exponential factors; E_i are the activation energies; R is the universal gas constant. The rate expressions for all reactions are given in Table 5.

Thus, for the first system we require 27 formal kinetic parameters k_{i0} , E_i , Q_i , and for the second – 24. Using

Table 3. Concentration designations for the Al + (Fe + Fe₂O₃) system

Таблица 3. Обозначения концентраций для системы $Al + (Fe + Fe_2O_3)$

| Species | Concentration | Species | Concentration | | |
|--------------------|---------------|----------------------------------|---------------|--|--|
| Al | C_1 | Fe ₂ Al ₅ | C_7 | | |
| Fe | C_2 | Al_2O_3 | C_8 | | |
| FeAl | C_3 | Fe_2O_3 | C_9 | | |
| FeAl ₂ | C_4 | FeO | C_{10} | | |
| Fe ₃ Al | C_5 | O_2 | C_{11} | | |
| FeAl ₃ | C_6 | FeAl ₂ O ₄ | C_{12} | | |

published parameters for overall reactions in SHS-type mixtures [21] is not feasible. One reason is the strong dependence of parameters on the determination method, mixture processing, heating rate, etc. Another is the lack of data for most steps. Even for one of the most studied thermite mixtures (Al–Fe₂O₃), published values are inconsistent [22], including the reaction enthalpies. For example, for reaction (VI) in the Al-containing system, [23] gives: $\Delta H = -851.4$ kJ/mol, whereas [16] reports $\Delta H \approx -752$ kJ/mol.

The entropies and enthalpies of reactions were obtained using Hess's law:

$$\Delta H_{298}^{0} = \sum_{\text{products}} v_{ki} \Delta H_{298}^{0} - \sum_{\text{reagents}} v_{ki} \Delta H_{298}^{0}, \qquad (9)$$

$$\Delta S_{298}^{0} = \sum_{\text{products}} v_{ki} \Delta S_{298}^{0} - \sum_{\text{reagents}} v_{ki} \Delta S_{298}^{0}, \qquad (10)$$

where the first terms on the right-hand side are sums of the parameters for the reaction products, and the second terms are the parameters for the reactants (reagents in the formula). However, tabulated values

Table 4. Concentration designations for the Ti + $(Fe_2O_3 + Fe + C)$ system

Таблица 4. Обозначения концентраций для системы $Ti + (Fe_2O_3 + Fe + C)$

| Species | Concentration | Species | Concentration |
|--------------------------------|---------------|----------------------------------|---------------|
| Ti | C_1 | TiFe ₂ | C_7 |
| Fe | C_2 | TiC | C_8 |
| Fe ₂ O ₃ | C_3 | FeO | C_9 |
| TiO ₂ | C_4 | O_2 | C_{10} |
| TiFe | C_5 | Ti ₃ FeO ₂ | C_{11} |
| Ti ₂ Fe | C_6 | | |

Table 5. Reaction rate expressions
Таблица 5. Скорости реакций

| Al-containing system | Reaction rate | Ti-containing system | Reaction rate | | |
|--|-------------------------------|---|----------------------------|--|--|
| 1) Al + Fe = FeAl | $\Phi_1 = k_1 C_1 C_2$ | 1) $3\text{Ti} + 2\text{Fe}_2\text{O}_3 = 3\text{TiO}_2 + 4\text{Fe}$ | $\Phi_1 = k_1 C_1^3 C_3^2$ | | |
| 2) $FeAl + Al = FeAl_2$ | $\Phi_2 = k_2 C_1 C_3$ | 2) Ti + Fe = TiFe | $\Phi_2 = k_2 C_1 C_2$ | | |
| $3) FeAl + 2Fe = Fe_3Al$ | $\Phi_3 = k_3 C_2^2 C_3$ | 3) $TiFe + Ti = Ti_2Fe$ | $\Phi_3 = k_3 C_1 C_5$ | | |
| $4) \operatorname{FeAl}_2 + \operatorname{Al} = \operatorname{FeAl}_3$ | $\Phi_4 = k_4 C_1 C_4$ | 4) $TiFe + Fe = TiFe_2$ | $\Phi_4 = k_4 C_2 C_5$ | | |
| $5) \operatorname{FeAl}_2 + \operatorname{FeAl}_3 = \operatorname{Fe}_2 \operatorname{Al}_5$ | $\Phi_5 = k_5 C_4 C_6$ | 5) Ti + C = TiC | $\Phi_5 = k_5 C_1 C_8$ | | |
| 6) $2Al + Fe_2O_3 = Al_2O_3 + 2Fe$ | $\Phi_6 = k_6 C_1^2 C_9$ | $6) 2 \text{Fe}_2 \text{O}_3 \rightarrow 4 \text{FeO} + \text{O}_2$ | $\Phi_6 = k_6 C_3^2$ | | |
| 7) $2\text{Fe}_2\text{O}_3 \rightarrow 4\text{FeO} + \text{O}_2$ | $\Phi_7 = k_7 C_9^2$ | 7) $Ti + O_2 = TiO_2$ | $\Phi_7 = k_7 C_1 C_{11}$ | | |
| 8) $FeO + Al_2O_3 = FeAl_2O_4$ | $\Phi_8 = k_8 C_9 C_{10}$ | 8) $TiO_2 + Ti_2Fe = Ti_3FeO_2$ | $\Phi_8 = k_8 C_4 C_6$ | | |
| 9) $4A1 + 3O_2 = 2Al_2O_3$ | $\Phi_9 = k_9 C_1^4 C_{11}^3$ | | | | |



are not available in the literature for all compounds. For this reason, approximate semi-empirical methods were used to obtain preliminary estimates of the formal kinetic parameters (Table 6). The parameter-estimation procedure is described in detail in [15].

For each system, the problem (which comprised 10 and 9 ordinary differential equations of the form (6) for the Al- and Ti-containing systems, respectively, plus the heat-balance equation (1)) was solved numerically using a semi-implicit Euler method. In every run, mass conservation and atomic balance were verified. Calculations were performed at constant ΔS_{298}^0 and ΔH_{298}^0 . The reaction orders were adjusted during the numerical solution. For the first system, we obtained:

$$\begin{split} k_{01} &= 10^{17}, \, k_{02} = 10^{22}, \, k_{03} = 3 \cdot 10^{22}, \, k_{04} = 10^{22}, \\ k_{05} &= 10^{22}, \, k_{06} = 8 \cdot 10^{19}, \, k_{07} = 6 \cdot 10^{15}, \\ k_{08} &= 10^{15}, \, k_{09} = 10^{24} \, \mathrm{s}^{-1}. \end{split}$$

For the second system, the adjustments affected two pre-exponential factors and the activation energy of one reaction:

$$k_{05} = 3 \cdot 10^{19} \text{ c}^{-1}, k_{06} = 6 \cdot 10^{23} \text{ s}^{-1},$$

$$E_6 = 150,255 \text{ J/mol}.$$

A single scaling factor applied to all reactions was 10^{-17} for the Al-containing system and $7.5 \cdot 10^{-13}$ for the Ti-containing system. The criterion for selecting this factor was the characteristic reaction time under the experimental conditions.

2.3. Numerical analysis results

Calculated temperature and composition profiles for reactive sintering of the studied systems are shown in Figs. 5–7. The typical temperature curves differ for the Al- and Ti-containing mixtures (Fig. 5). In the former, a temperature spike appears upon reaction initiation at T = 700-900 K. In the latter, there is no pronounced spike, although a wavy temperature curve is observed.

Such behavior is often ascribed to thermocouple sensitivity; however, the calculations indicate that it may also arise from the interplay of coupled physicochemical processes.

As noted above, the exact oxide composition in the chips is unknown. Accordingly, the modeling allows for different choices of initial data (Table 7). We assume the presence of two iron oxides – FeO and Fe₂O₃. Fe₃O₄ can, to first approximation, be treated as a combination of FeO and Fe₂O₃ and is therefore not included explicitly. In addition, the numerical experiment accounts for adsorbed oxygen and alumina on particle surfaces. Only under this assumption does the model reproduce the amount of Al₂O₃ observed experimentally in the products. The numerical study further enables exploration over a wide range of initial compositions, which is difficult to achieve experimentally.

No such complications arose for the Ti system, although the initial composition of the powder mixture can likewise be varied numerically.

Composition-evolution results for different initial data are presented in Figs. 6 and 7. We find that

Table 6. Formal kinetic parameters obtained using a semi-empirical approach
Таблица 6. Формально-кинетические параметры, найденные с помощью полуэмпирического подхода

| | $Al + (Fe + Fe_2O_3)$ | | | | | $Ti + (Fe_2O_3 + Fe + C)$ | | | | | |
|--------------|-----------------------|-------------------|-----------|--------------------|--------------|---------------------------|-------------|-----------|--------------------|--|--|
| Reaction No. | ΔS_{298}^0 | k_{0i} | E | ΔH_{298}^0 | Reaction No. | ΔS_{298}^0 | k_{0i} | E | ΔH_{298}^0 | | |
| 1 | -26.10 | 1015 | 32,104.53 | -30.7 | 1 | -0.36 | 9.1013 | 15,710.04 | -1155.0 | | |
| 2 | -25.15 | 1015 | 31,218.18 | -33.7 | 2 | -3.47 | 1014 | 18,730.20 | -44.6 | | |
| 3 | -36.10 | 3.1015 | 36,638.25 | -93.0 | 3 | -40.92 | 1016 | 78,275.70 | -49.1 | | |
| 4 | -26.38 | 1015 | 32,365.77 | -37.6 | 4 | -40.43 | 1016 | 77,496.60 | -45.4 | | |
| 5 | -24.95 | 1015 | 47,960.92 | -161.5 | 5 | -161.62 | 3.1022 | 17,970.00 | -209.0 | | |
| 6 | -38.48 | 8.1015 | 43,655.07 | -760.0 | 6 | 274.20 | 6.10^{26} | 15,255.54 | 584.0 | | |
| 7 | 274.30 | $6 \cdot 10^{26}$ | 15,260.94 | 584.0 | 7 | -183.32 | 1022 | 10,348.02 | -933.0 | | |
| 8 | -5.40 | 1014 | 22,621.50 | -122.0 | 8 | 10.60 | 2.1014 | 32,147.00 | -173.3 | | |
| 9 | -626.86 | 1045 | 34,299.18 | -3164.0 | | | | | | | |

N o t e s . Units: $[\Delta S_{298}^0] = J/(\text{mol} \cdot K)$; $[k_{0i}] = \text{s}^{-1}$; [E] = J/mol; $[\Delta H_{298}^0] = \text{kJ/mol}$. Reaction numbers follow Table 5.



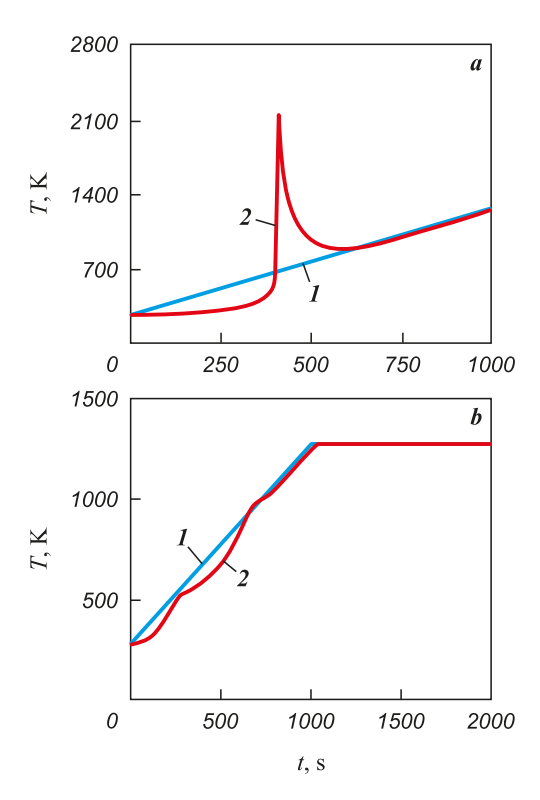


Fig. 5. Typical temperature curves for the composition with (a) and titanium (b)

Mixtures compositions 2 from Table 7 Sintering temperature $T_s = 1273$ K I – heater temperature; 2 – sample temperature

Рис. 5. Типичное поведение температурных кривых для состава с алюминием (a) и титаном (b)

Составы смесей 2 из табл. 7 Температура спекания $T_{\rm s}=1273~{
m K}$ I – температура нагревателя; 2 – температура образца

the product composition can vary substantially. For the Al-containing system (Fig. 6), the products always contain Fe_3Al and $FeAl_3$ intermetallics in different proportions, as well as Al_2O_3 . The reduction of iron is the fastest reaction. FeAl is not observed in the products. The mixed oxide appears only when the initial mixture contains Al_2O_3 , FeO, and oxygen; in that case, Fe_2Al_5 is also present. The experimental data are best matched by Composition 2, which includes oxygen and oxide in the starting mixture.

The phase composition of the Ti compact also evolves (Fig. 7). All reactions proceed actively over a time interval shorter than the total sintering time. For all initial compositions, the products always contain the intermetallic Ti₂Fe and unreacted Ti. TiFe appears as an intermediate during sintering. In three variants, the product contains Ti₃FeO₂. In the second variant, the starting mixture contains a small amount of iron oxide, hence its role is minor; however, Fe₂O₃ most closely reflects the experimental conditions. Under the experimental conditions, the product con-

tains 91 wt. % of α -Ti solid solution + Ti₂Fe and α -Ti solid solution + TiFe. In this case, Fe₂O₃ is insufficient to form TiO₂. In the other three variants, TiO₂ appears as an intermediate that is consumed rapidly to form the complex oxide.

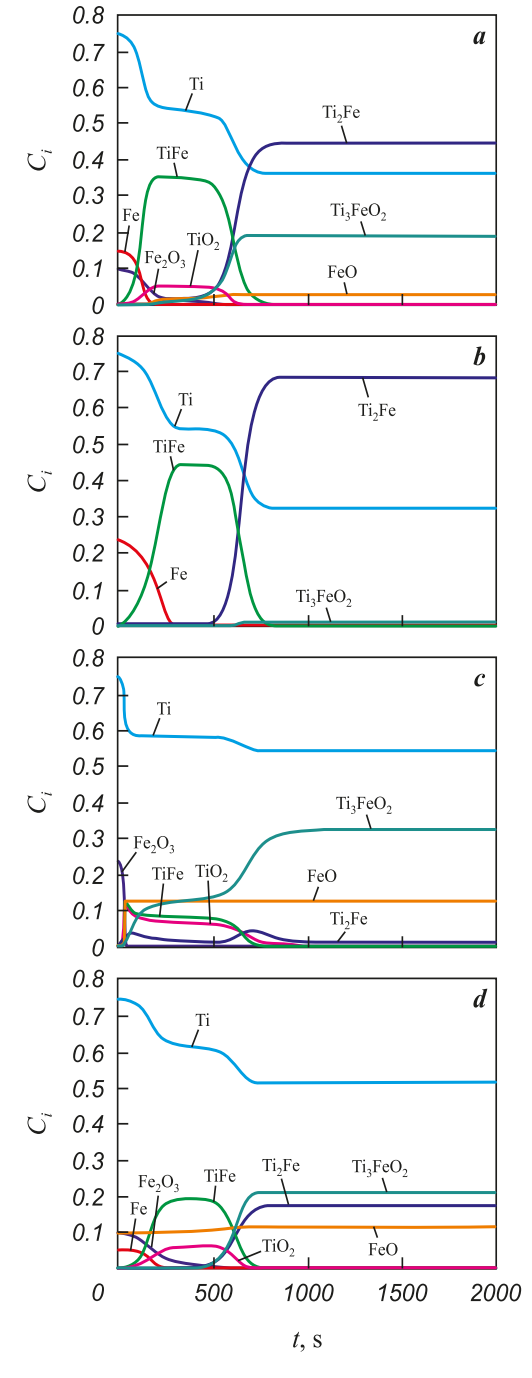


Fig. **6.** Phase composition evolution of the aluminium compact during sintering The nitial composition corresponds to Table 7 Al-based mixtures: a – composition l, b – 2, c – 3, d – 4

Рис. 6. Изменение фазового состава прессовки с алюминием в условиях спекания Начальный состав соответствует табл. 7 Составы с Al: a – состав l, b – 2, c – 3, d – 4



| Table 7. Initial data for calculations |
|---|
| <i>Таблица 7.</i> Начальные данные для расчетов |

| Composition No. (numerical | Initial composition of the Al-containing mixture, wt. % | | | | | | | Initial composition of the Ti-containing mixture, % | | | |
|----------------------------|---|--------------------------------|------|------|----------------|--------------------------------|------|---|-------|------|-------|
| experiment) | Al | Fe ₂ O ₃ | Fe | FeO | O ₂ | Al ₂ O ₃ | Ti | Fe ₂ O ₃ | Fe | FeO | С |
| 1 | 0.25 | 0.45 | 0.30 | _ | ı | _ | 0.75 | 0.100 | 0.150 | _ | _ |
| 2 | 0.25 | 0.20 | 0.30 | 0.15 | 0.05 | 0.05 | 0.75 | 0.010 | 0.239 | _ | 0.001 |
| 3 | 0.25 | 0.15 | 0.30 | 0.20 | 0.50 | 0.05 | 0.75 | 0.239 | 0.010 | _ | 0.001 |
| 4 | 0.60 | 0.20 | 0.20 | _ | _ | _ | 0.75 | 0.100 | 0.050 | 0.10 | _ |

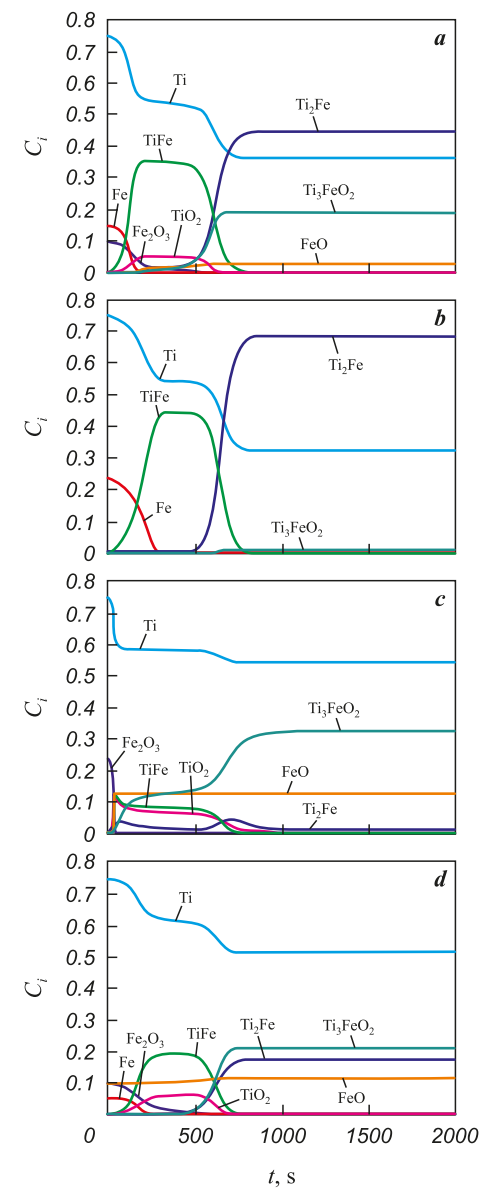


Fig. 7. Phase composition evolution of the titanium compact during sintering The initial composition corresponds to Table 7 Ti-based mixtures: a – composition 1, b – 2, c – 3, d – 4

Рис. 7. Изменение фазового состава прессовки с титаном в условиях спекания

Начальный состав соответствует табл. 7 Составы с Ті: a – состав l, b – 2, c – 3, d – 4

Conclusion

This study demonstrates good agreement between the proposed thermokinetic model and experimental data for multicomponent powder mixtures – recycled steel-chip powder with aluminum or titanium – under vacuum sintering. Consistent with the experiments, the calculations predict substantial heat release upon heating $Al + (Fe + Fe_2O_3 + C)$ mixtures, whereas $Ti + (Fe + Fe_2O_3 + C)$ sinters in a steady regime. In the former case, aluminum carbide was not included in the model because of the low sintering temperature; in the latter, titanium carbide formed only in trace amounts. No carbides were detected experimentally in either system.

References / Список литературы

- Yeh C.L., Li R.F. Formation of TiAl-Ti₅Si₃ and TiAl-Al₂O₃ in situ composites by combustion synthesis. *Intermetallics*. 2008;16(1):64–70. https://doi.org/10.1016/j.intermet.2007.07.016
- Zhang X., Li X., Wang J., Liu L., Li S., Li B., Hou X., Gao J., Kariya S., Umeda J., Kondoh K., Li S. Synthesis mechanism and interface contribution towards the strengthening effect of *in-situ* Ti₅Si₃ reinforced Al matrix composites. *Materials Science and Engineering: A.* 2024; 918:147427. https://doi.org/10.1016/j.msea.2024.147427
- **3.** Yang Y.F., Mu D.K., Jiang Q.C. A simple route to fabricate TiC–TiB₂/Ni composite via thermal explosion reaction assisted with external pressure in air. *Materials Chemistry and Physics*. 2014;143(2):480–485.
- https://doi.org/10.1016/j.matchemphys.2013.10.003
 Lemboub S., Boudebane S., Gotor F.J., Haouli S., Mezrag S., Bouhedja S., Hesser G., Chadli H., Chouchane T. Core-rim structure formation in TiC–Ni based cermets fabricated by a combined thermal explosion/hot-pressing process. *International Journal of Refractory Metals and Hard Materials*. 2018;70:84–92.
 - https://doi.org/10.1016/j.ijrmhm.2017.09.014
- 5. Yeh C.L., Ke C.Y. Synthesis of TiB₂–Al₂O₃–FeAl composites via self-sustaining combustion with Fe₂O₃/TiO₂-based thermite mixtures. *Ceramics International*. 2018;44(13): 16030–16034.
 - https://doi.org/10.1016/j.ceramint.2018.06.040

Knyazeva A.G., Korosteleva E.N., Safronova V.S. Sintering and thermokinetic modeling ...

- **6.** Zhang K., Fen W., Zhu J., Wu H. Mechanical properties and microstructure of Al₂O₃/TiAl *in situ* composites doped with Cr and V₂O₅. *Science of Sintering*. 2012;44(1):73–80. https://doi.org/10.2298/SOS1201073Z
- Motlagh E.B., Nasiri H., Khaki J.V., Sabzevar M.H. Formation of metal matrix composite reinforced with nano sized Al₂O₃+Ni–Al intermetallics during coating of Al substrate via combustion synthesis. Surface & Coatings Technology. 2011;205(23-24):5515–5520. https://doi.org/10.1016/j.surfcoat.2011.06.026
- Kim J.-W., Lee J.-M., Lee J.-H., Lee J.-C. Role of excess Al on the combustion reaction in the Al–TiO₂–C system. *Metals and Materials International*. 2014;20(6): 1151–1156. https://doi.org/10.1007/s12540-014-6020-8
- Miloserdov P.A., Gorshkov V.A., Andreev D.E., Yukhvid V.I., Miloserdova O.M., Golosova O.A. Metallothermic SHS of Al₂O₃-Cr₂O₃ + TiC ceramic composite material. *Ceramics International*. 2023;49(14):24071–24076. https://doi.org/10.1016/j.ceramint.2023.04.145
- **10.** Korosteleva E.N., Knyazeva A.G., Nikolaev I.O. Phase formation in reactive sintering with reduction. *Physical Mesomechanics*. 2023;26(1):39–47. https://doi.org/10.1134/S1029959923010058
- 11. Korosteleva E.N., Nikolaev I.O. Evolution of the structural-phase state of steel swarf during its processing into a powdered product. *Powder Metallurgy and Functional Coatings*. 2024;18(4):6–16. https://doi.org/10.17073/1997-308X-2024-4-6-16
 - Коростелева Е.Н., Николаев И.О. Эволюция структурно-фазового состояния стальной стружки в процессе ее переработки в порошкообразный продукт. Известиия вузов. Порошковая металлургия и функциональные покрытия. 2024;18(4):6–16.
 - https://doi.org/10.17073/1997-308X-2024-4-6-16
- 12. Korosteleva E.N., Nikolaev I.O., Baranovsky A.V. Synthesis and evolution of the structural and phase state of powder materials Al–Fe–Fe₂O₃ under heating conditions. In: *Collection of materials of the XVII Minsk International Heat and Mass Transfer Forum* (20–24 May 2024). Minsk: Institute of Heat and Mass Transfer n.a. Lykov of the NAS of Belarus, 2024. P. 746–748. (In Russ.).
 - Коростелева Е.Н., Николаев И.О., Барановский А.В. Синтез и эволюция структурно-фазового состояния порошковых материалов Al–Fe–Fe₂O₃ в условиях нагрева. В сб.: *Материалы XVII Минского международного форума по тепло- и массообмену* (20–24 мая 2024 г.). Минск: Институт тепло- и массообмена им. А.В. Лыкова НАН Беларуси, 2024. С. 746–748.
- **13.** Miedema A.R., de Châtel P.F, de Boer F.R., de Chatel P.F. Cohesion in alloys fundamental of a semi-empirical model. *Physica B* + *C*. 1980;100(1):1–28. https://doi.org/10.1016/0378-4363(80)90054-6

- **14.** Binnewies M., Milke E. Thermochemical data of elements and compounds. Wiley-VCH Verlag GmbH, 2008. 928 p. https://doi.org/10.1002/9783527618347
- 15. Safronova V.S., Knyazeva A.G., Korosteleva E.N. A theoretical and experimental study of phase formation in Ti–CuO powder mixtures under reactive sintering conditions. *New Journal of Chemistry*. 2025;49(3):893–909. https://doi.org/10.1039/d4nj03751k
- Podergin V.A. Metallothermal systems. Moscow: Metallurgiya, 1992. 272 p. (In Russ.).
 - Подергин В.А. Металлотермические системы. М.: Металлургия, 1992. 272 с.
- 17. Korchagin M.A., Podergin V.A. Investigation of chemical transformations in the combustion of condensed systems. *Combustion, Explosion, and Shock Waves*. 1979;15(3):325–329.
 - https://doi.org/10.1007/BF00785065
 - Корчагин М.А., Подергин В.А. Исследование химических превращений при горении конденсированных систем. *Физика горения и взрыва*. 1979;(3):48–53.
- **18.** Liu W., Ismail M., Dunstan M.T., Hu W., Zhang Z., Fennell P.S., Scott S.A., Dennis J.S. Inhibiting the interaction between FeO and Al₂O₃ during chemical looping production of hydrogen. *RSC Advances*. 2015;5(3):1759–1771. https://doi.org/10.1039/C4RA11891J
- 19. Liu Y., Watanabe M., Okugawa M., Hagiwara T., Sato T., Seguchi Y., Adachi Y., Minamino Y., Koizumi Y. Resolving the long-standing discrepancy in Fe₃Al ordering mobilities: A synergistic experimental and phase-field study. Acta Materialia. 2024;273:119958. https://doi.org/10.1016/j.actamat.2024.119958
- Lin Y.-C., Shteinberg A.S., McGinn P.J., Mukasyan A.S. Kinetics study in Ti–Fe₂O₃ system by electro-thermal explosion method. *International Journal of Thermal Sciences*. 2014;84:369–378.
 - https://doi.org/10.1016/j.ijthermalsci.2014.06.008
- **21.** Mukasyan A.S., Shuck C.E. Kinetics of SHS reactions: A review. *International Journal of Self-Propagating High-Temperature Synthesis*. 2017;26(3):145–165. https://doi.org/10.3103/S1061386217030049
- **22.** Durães L., Costa B.F.O., Santos R., Correia A., Campos J., Portugal A. Fe₂O₃/aluminum thermite reaction intermediate and final products characterization. *Materials Science and Engineering: A.* 2007;465(1-2):199–210. https://doi.org/10.1016/j.msea.2007.03.063
- 23. Bodaghi M., Zolfonoon H., Tahriri M., Karimi M. Synthesis and characterization of nanocrystalline α-Al₂O₃ using Al and Fe₂O₃ (hematite) through mechanical alloying. *Solid State Sciences*. 2009;11(2):496–500. https://doi.org/10.1016/j.solidstatesciences.2008.06.021

Information about the Authors



Сведения об авторах

Anna G. Knyazeva – Chief Researcher, Laboratory of Nonlinear Mechanics of Metamaterials and Multilevel Systems, Institute of Strength Physics and Materials Science, Siberian Branch of the Russian Academy of Sciences (ISPMS SB RAS)

(i) *ORCID*: 0000-0002-9765-7695 **☑** *E-mail*: anna-knyazeva@mail.ru

Elena N. Korosteleva – Senior Researcher, Laboratory of Physics of Powder Materials Consolidation of the ISPMS SB RAS

ORCID: 0000-0002-4363-3604
 E-mail: elenak@ispms.ru

Valeriya S. Safronova – Research Assistant, Laboratory of Nonlinear Mechanics of Metamaterials and Multilevel Systems of the ISPMS SB RAS

(D) ORCID: 0009-0004-7423-5897 **IIII** I9627826013@yandex.ru

Анна Георгиевна Князева – гл. науч. сотрудник лаборатории нелинейной механики метаматериалов и многоуровневых систем Института физики прочности и материаловедения (ИФПМ) СО РАН

ORCID: 0000-0002-9765-7695
 E-mail: anna-knyazeva@mail.ru

Елена Николаевна Коростелева – ст. науч. сотрудник лаборатории физики консолидации порошковых материалов ИФПМ СО РАН

(D) *ORCID*: 0000-0002-4363-3604 **⊠** *E-mail:* elenak@ispms.ru

Валерия Сергеевна Сафронова – лаборант-исследователь лаборатории нелинейной механики метаматериалов и многоуровневых систем ИФПМ СО РАН

ြ ORCID: 0009-0004-7423-5897 **☑ E-mail:** l9627826013@yandex.ru

Contribution of the Authors



Вклад авторов

A. G. Knyazeva – development of the main concept, formulation of the research objectives and tasks, model formulation, preparation of the text, and formulation of conclusions.

E. N. Korosteleva – experimental testing of the samples and preparation of the manuscript.

V. S. Safronova – development of the computational program, performing calculations, and analysis of the research results.

А. Г. Князева – формирование основной концепции, постановка цели и задачи исследования, формулировка модели, подготовка текста, формулировка выводов.

Е. Н. Коростелева – проведение испытаний образцов, подготовка текста статьи.

В. С. Сафронова – написание программы, проведение расчетов, анализ результатов исследований.

Received 23.03.2025 Revised 24.04.2025 Accepted 28.04.2025 Статья поступила 23.03.2025 г. Доработана 24.04.2025 г. Принята к публикации 28.04.2025 г.